

Single-cell deep phenotyping of IgG-secreting cells for high-resolution immune monitoring

Klaus Eyer¹, Raphaël C L Doineau^{2,3,7}, Carlos E Castrillon^{4,5,7}, Luis Briseño-Roa^{3,6} , Vera Menrath³, Guillaume Mottet^{4,5}, Patrick England⁶, Alexei Godina^{2,6}, Elodie Briant-Litzler^{2,6}, Clément Nizak² , Allan Jensen³, Andrew D Griffiths^{2,8}, Jérôme Bibette¹, Pierre Bruhns^{4,5,8}  & Jean Baudry^{1,8} 

Studies of the dynamics of the antibody-mediated immune response have been hampered by the absence of quantitative, high-throughput systems to analyze individual antibody-secreting cells^{1–5}. Here we describe a simple microfluidic system, DropMap, in which single cells are compartmentalized in tens of thousands of 40-pL droplets and analyzed in two-dimensional droplet arrays using a fluorescence relocation-based immunoassay. Using DropMap, we characterized antibody-secreting cells in mice immunized with tetanus toxoid (TT) over a 7-week protocol, simultaneously analyzing the secretion rate and affinity of IgG from over 0.5 million individual cells enriched from spleen and bone marrow. Immunization resulted in dramatic increases in the range of both single-cell secretion rates and affinities, which spanned at maximum 3 and 4 logs, respectively. We observed differences over time in dynamics of secretion rate and affinity within and between anatomical compartments. This system will not only enable immune monitoring and optimization of immunization and vaccination protocols but also potentiate antibody screening^{6,7}.

B cells and the antibodies they secrete are a critical arm of the immune response. Antibodies are classified into several isotypes; IgG is the main type of antibody found in blood and extracellular fluid and enables control of infection. The levels of antigen-specific IgG in circulating blood correlate with an individual's immunological history⁸, and the average affinity of antibodies for their target tends to increase during an immune response⁹. Mass spectrometry of circulating IgG coupled with next-generation sequencing has recently been used to gain further insights at the molecular level^{10,11}. However, this approach does not capture a complete picture of the complexity of the humoral immune response and serum IgG composition, which is a function of the frequency of IgG-secreting cells (IgG-SCs), their IgG secretion rates, and the affinity of the secreted IgGs for the antigen. The pool of IgG-SCs is heterogeneous and consists mainly of plasmablasts and

short-lived plasma cells in the spleen and long-lived plasma cells in the bone marrow⁸, but each individual IgG-SC is unique and produces only one IgG variant¹². Therefore, a direct and statistical analysis of individual IgG-SCs would provide a more profound understanding of the immune response.

Functional analysis of cloned, immortalized IgG-SCs and myeloma cells has allowed quantitative measurement of average secretion rates, affinities and specificities of antibodies, but usually only from a small number of clones (typically <10²)^{1–5}. In contrast, next-generation sequencing allows the molecular identification of large numbers of expressed antibody genes¹³, but subsequent cloning and expression are needed to determine phenotypic properties such as the affinity and specificity of the antibodies, a process that is laborious and low-throughput¹⁴. For the large-scale phenotypic characterization of IgG-SC populations, tens of thousands of non-immortalized IgG-SCs can be screened using enzyme-linked immunospot (ELISPOT) or related assays^{15–17}, or by compartmentalization in microfabricated arrays^{18,19}, to detect antibody secretion and antigen binding. Compartmentalization of individual cells in picoliter droplets²⁰ has also been used for high-throughput screening and sorting of hybridoma cells based on the binding or inhibitory activity of secreted antibodies^{6,7}. However, none of these methods allows quantitative, sensitive, and simultaneous real-time kinetic measurement of antibody secretion rate and affinity at the single-cell level, rendering impossible a deep and quantitative assessment of the phenotypical complexity and variability of IgG-SC populations following immunization or vaccination.

We describe here a droplet-based microfluidic technology (DropMap) that overcomes previous limitations. The combination of immobilizing ('parking') picoliter-size droplets and a fast and ultrasensitive bioassay allows massively parallel kinetic analyses of single IgG-SCs, with simultaneous measurement of antibody secretion rate, specificity, and affinity for the antigen. We used this system to characterize the humoral response in mice immunized with TT over a 7-week protocol, producing a quantitative, statistical analysis

¹Laboratoire Colloïdes et Matériaux Divisés (LCMD), ESPCI Paris, PSL Research University, CNRS UMR8231 Chimie Biologie Innovation, Paris, France. ²Laboratoire de Biochimie (LBC), ESPCI Paris, PSL Research University, CNRS UMR8231 Chimie Biologie Innovation, Paris, France. ³HiFiBio SAS Paris, France. ⁴Unit of Antibodies in Therapy and Pathology, Department of Immunology, Institut Pasteur, Paris, France. ⁵INSERM, Paris, France. ⁶Present addresses: Alexion R&D France, Institut Imagine, Paris, France (L.B.-R.), Plateforme de Biophysique Moléculaire, Centre d'Innovation et Recherche Technologique (Citech), Institut Pasteur, Paris, France (P.E.), TOTAL New Energies, RD Biotechnologies, Paris, France (A.G.) and Centre d'Innovation et Recherche Technologique (Citech), Institut Pasteur, Paris, France (E.B.-L.). ⁷These authors contributed equally to this work. ⁸These authors jointly supervised this work. Correspondence should be addressed to A.D.G. (andrew.griffiths@espci.fr), P.B. (pierre.bruhns@pasteur.fr), J.B. (jean.baudry@espci.fr).

Received 12 October 2016; accepted 17 August 2017; published online 11 September 2017; doi:10.1038/nbt.3964

of the distribution of secretion rates and affinities over the course of an immune response.

The DropMap technology is based on kinetic analysis of droplets immobilized in a two-dimensional (2D) array (Fig. 1a, **Supplementary Notes** and supplementary fig. 1)²¹. Single cells were compartmentalized in monodisperse 40-pL aqueous droplets in inert fluorinated carrier oil by hydrodynamic flow focusing in a microfluidic system²². Cells and assay reagents were brought together on the microfluidic chip just before droplet creation, with the cells diluted to give an average of 0.2–0.4 cells per droplet for the encapsulation of up to one cell per drop. Droplets were immobilized by a slight physical confinement in the *z*-direction within the chamber (<15%), allowing them to be observed over time. In this study, 40,000 droplets (i.e., 8,000–16,000 individual cells) were imaged over an area of 8.6 × 6.5 mm (**Supplementary Notes**).

To quantify IgG, we devised an in-droplet sandwich immunoassay based on paramagnetic nanoparticles (Fig. 1b). The nanoparticles were pre-coated with an anti-mouse kappa light-chain (Igκ) nanobody (V_{HH}) to capture secreted immunoglobulin. The ~1,300 nanoparticles in each drop were induced to form an elongated, observable aggregate, termed a beadline, by applying a magnetic field. Compared to previous approaches relying on the co-encapsulation of a single cell and a single 6-μm bead⁷, the use of nanoparticles increased the antibody binding capacity and lowered the number of droplets containing no beads, which improved the performance of the assay (**Supplementary Notes**, supplementary fig. 2). Each droplet also contained Alexa647-labeled F(ab')₂ specific for mouse IgG Fc (termed anti-IgG(Fc), red fluorescent) and Alexa488-labeled antigen (here TT) (green fluorescent) (Fig. 1c and **Supplementary Notes**, supplementary fig. 3). IgG and anti-IgG(Fc) were captured onto the beadline, and the concentration of IgG was determined from the ratio of red fluorescence on the beadline to mean fluorescence within the droplet. Our calibration curve (Fig. 1d) was based on a purified anti-TT IgG (TT7) with K_d of 8 nM (**Supplementary Notes**). In this calibration, increasing concentrations of TT7 resulted in an increase in red fluorescence (anti-IgG(Fc)) relocation on the beadline up to a concentration of around 75 nM (Fig. 1d and **Supplementary Notes**, supplementary fig. 2), then a decrease as the binding capacity of the nanoparticles was exceeded. The same general behavior was seen with green fluorescence (Alexa488-labeled TT) relocation, although saturation occurred at a slightly lower concentration (~40 nM; Fig. 1d). These results closely fit the theoretical model (**Supplementary Notes**, supplementary figs. 3 and 4, and supplementary table 1). Secretion rates were calculated by measuring the change in IgG concentration over time (Fig. 1e). IgG secretion in droplets of pL volume reached nM range concentrations in about 30 min, allowing quantitative measurement via the relocation immunoassay. Secretion rates were precisely determined from ~4 to 10,000 IgG/s, a dynamic range that is in accordance with secretion rates reported in the literature^{8–11}. Cells were defined as IgG-SCs if the secretion rate exceeded 4 IgG/s, which was determined to be the lower limit of detection within the timeframe of an experiment (see also **Supplementary Notes**, supplementary figs. 5–7 for further controls).

If the secreted IgG recognizes the antigen (here TT), the ratio of antigen (green fluorescent) bound to IgG on the beadline and the mean fluorescence within the droplet can be used to calculate the strength of the interaction (K_d), because the concentration of IgG is measured and that of antigen is imposed (**Supplementary Notes**). The K_d is determined from the slope of the line defined by plotting the relocation of red fluorescent anti-IgG(Fc), versus the relocation of green fluorescent antigen to the beadline at different

concentrations of IgG (≤50 nM) (Fig. 1e). These curves are plotted using the experimental data at IgG concentration ≤50 nM for the anti-TT antibody TT7 and an anti-CD34 antibody, which does not bind TT (Fig. 1f). Slopes were determined for a panel of seven purified anti-TT IgGs and plotted versus the K_d values (Fig. 1g), which ranged from 300 to 0.02 nM (determined using surface plasmon resonance (SPR); **Supplementary Notes**, supplementary table 2). The results are in agreement with the theoretical model (**Supplementary Notes**, supplementary fig. 4d), and show that the assay has a dynamic range of ~4 logs, spanning the typical range of affinities found for humoral responses^{23,24}.

Five of those anti-TT IgGs, with K_d values ranging from 150 to 0.6 nM, were also expressed from individual Chinese hamster ovary (CHO) cells (3 IgGs) and human embryonic kidney (HEK293T) cells (2 IgGs). The mean IgG secretion rate measured in droplets was similar for the three stably transfected CHO lines (173 ± 12 IgG/s per cell) and close to that measured as an average in bulk, using homogeneous time-resolved fluorescence (192 ± 21 IgG/s per cell; see also **Supplementary Notes**). However, IgG secretion rates from single cells varied widely (~10 to ~900 IgG/s, CV 1.99), consistent with the wide variance in protein (including antibody) expression at the single-cell level previously described for CHO and other cell lines^{19,25,26}. The mean IgG secretion rates measured for the transiently transfected HEK293T cells were lower than for the CHO cells, but similar for the different antibodies (74 ± 51 IgG/s per cell; **Supplementary Notes**, supplementary fig. 8). For all five IgG-secreting cell lines, the mean K_d values measured in droplets closely approximated the values determined by bulk measurements using SPR (gold standard), with relatively similar coefficient of variation (CV; mean CVs 0.5 and 0.25, respectively; see **Supplementary Notes**, supplementary table 3 and Supplementary fig. 8). No significant correlation between the measured secretion rates and the measured K_d was observed (**Supplementary Notes**, supplementary table 4 for statistical analysis).

Next, we applied the DropMap system to follow anti-TT responses over time after primary (day 0) and secondary (day 14) immunizations in adjuvant, and a boost (day 42) without adjuvant. We harvested splenocytes and bone marrow cells from the same mouse, with three mice per time point (45 mice in total; **Supplementary Notes**, supplementary fig. 9). We analyzed a total of 575,553 B-cell lineage-enriched cells (~12,800 cells/mouse; see **Supplementary Notes** and **Supplementary Data 1** and **2** for numbers), simultaneously measuring IgG secretion rate and affinity for TT for each IgG-SC (**Supplementary Notes**).

Before immunization, the frequency of IgG-SCs was low (≤0.1%), but increased 80-fold in the spleen and 45-fold in the bone marrow, peaking 4–7 d after each immunization (Fig. 2a). Notably, the frequency of IgG-SCs with and without detectable TT-binding evolved similarly, with, on average, 17 ± 3% (relative s.e.m., as for all subsequent data) of IgG-SCs producing anti-TT antibodies in both anatomical compartments (Fig. 2b,c). The use of complete Freund's adjuvant, which contains mycobacterial antigens, may contribute to the high frequency of cells secreting IgGs without detectable TT-binding after the primary immunization, but it does not explain their high frequency after secondary immunization (with incomplete Freund's adjuvant) and boost (with no adjuvant).

Cells secreting polyspecific IgG (antibodies that non-specifically stick to the beadline and non-related antigens) were identified and excluded from data analysis (**Supplementary Notes**, supplementary fig. 11). The differences in frequencies of cells secreting non-TT-binding IgG and anti-TT IgG were minor between the three mice at each time point (Fig. 2a,b), indicating high reproducibility.

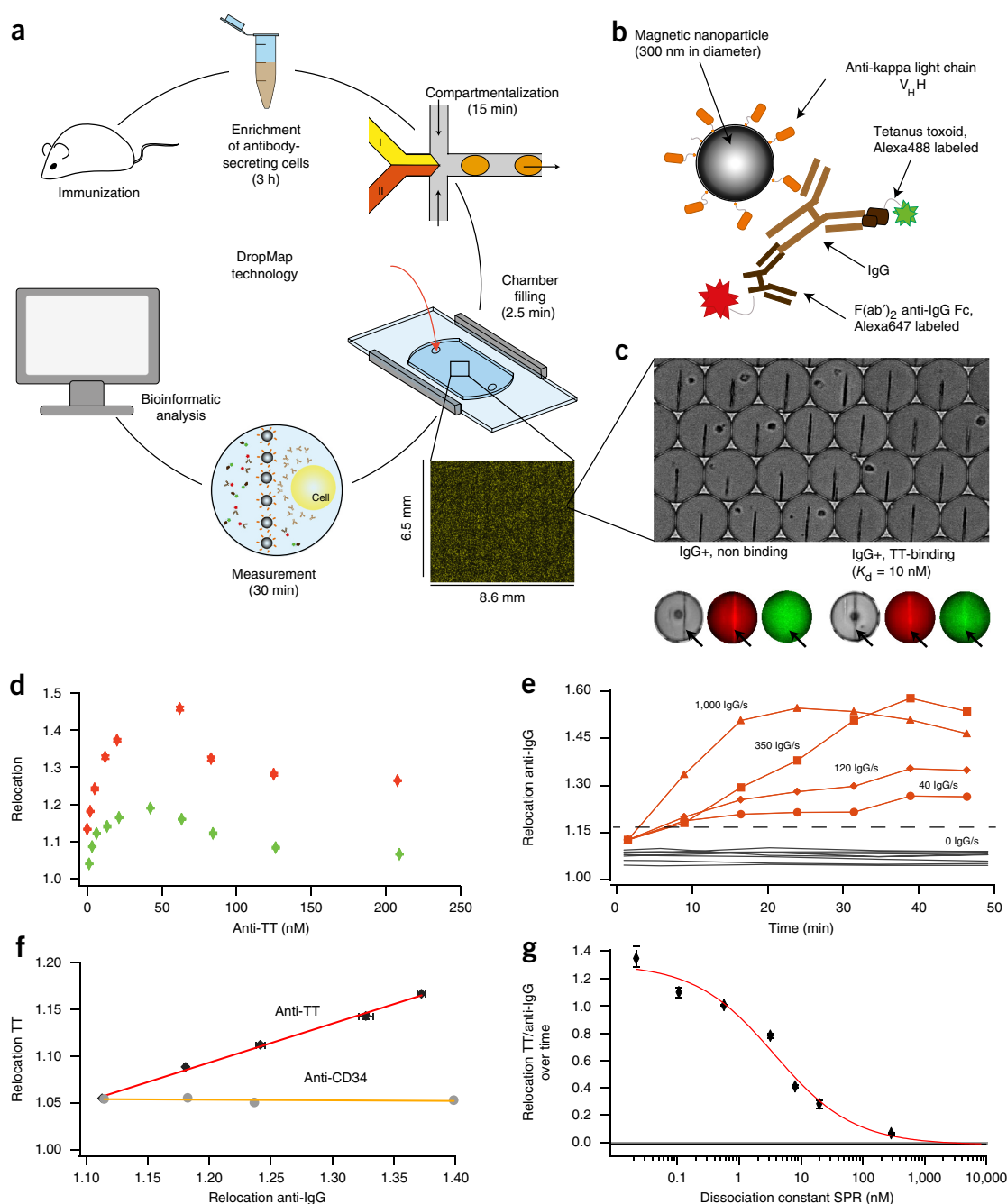


Figure 1 DropMap technology principle and calibration. **(a)** Overview of the workflow and timing. IgG-SCs were isolated and enriched from immunized mice, and compartmentalized in 40-pL droplets using a microfluidic device. Two aqueous phases (I and II), one containing cells or calibration antibodies (I) and the other containing paramagnetic nanoparticles and fluorescently labeled detection reagents (II). After creation, droplets were loaded into an observation chamber to form a 2D droplet array, flow was stopped, and the IgG secretion and affinity was measured over time. The insert shows 40,000 droplets, stained with different concentration of sulforhodamine B for visualization. **(b)** The bioassay comprises magnetic nanoparticles pre-coated with anti-mouse kappa light chain V_HH that captures antibodies onto the bead surface. Red fluorescent anti-IgG(Fc), binds to the IgG fraction of immobilized antibodies. If the immobilized IgG possesses affinity for the antigen (here TT), the (green fluorescent) antigen also relocates onto the bead surface. **(c)** At top, brightfield image of beadlines and splenocytes in an array of 40-pL droplets. To enable the measurement of fluorescence relocation onto the bead surface, the nanoparticles were cross-linked to form an observable micrometer-sized structure, the beadline, by applying a magnetic field. At bottom, the image series shows brightfield, red fluorescence and green fluorescence images for a non-binding (left) and TT-binding IgG (right), with the beadline indicated by a black arrow. **(d)** Relocation of anti-IgG(Fc), and TT (red and green, respectively) to the beadline as a function of the concentration of anti-TT IgG (TT7, K_d of 8 nM) in the presence of 75 nM anti-IgG(Fc), and 25 nM TT-Alexa488. **(e)** Relocation of the red fluorescent anti-IgG(Fc) was used to calculate secretion rates from individual splenic mouse B cells (orange, $n = 4$), shown in comparison to droplets containing no B cell (gray, $n = 8$). **(f)** Relocation of TT as a function of relocation of the red fluorescent anti-IgG(Fc), with different concentrations of an IgG with no affinity for TT (anti-CD34) and the anti-TT antibody TT7. **(g)** Plot of the slopes (see **f**), defined by change in relocation of TT divided by the change in relocation of anti-IgG, versus the dissociation constant (K_d) measured by SPR of seven TT-binding IgGs (black) and an antibody with no affinity for TT (horizontal line, anti-CD34, a cell surface glycoprotein). The data were fitted to the sigmoidal curve (red line) predicted by the model ($\chi^2 = 0.03$), which was subsequently used as a standard curve to calculate K_d values for IgGs secreted from single cells. Error bars represent the s.e.m.

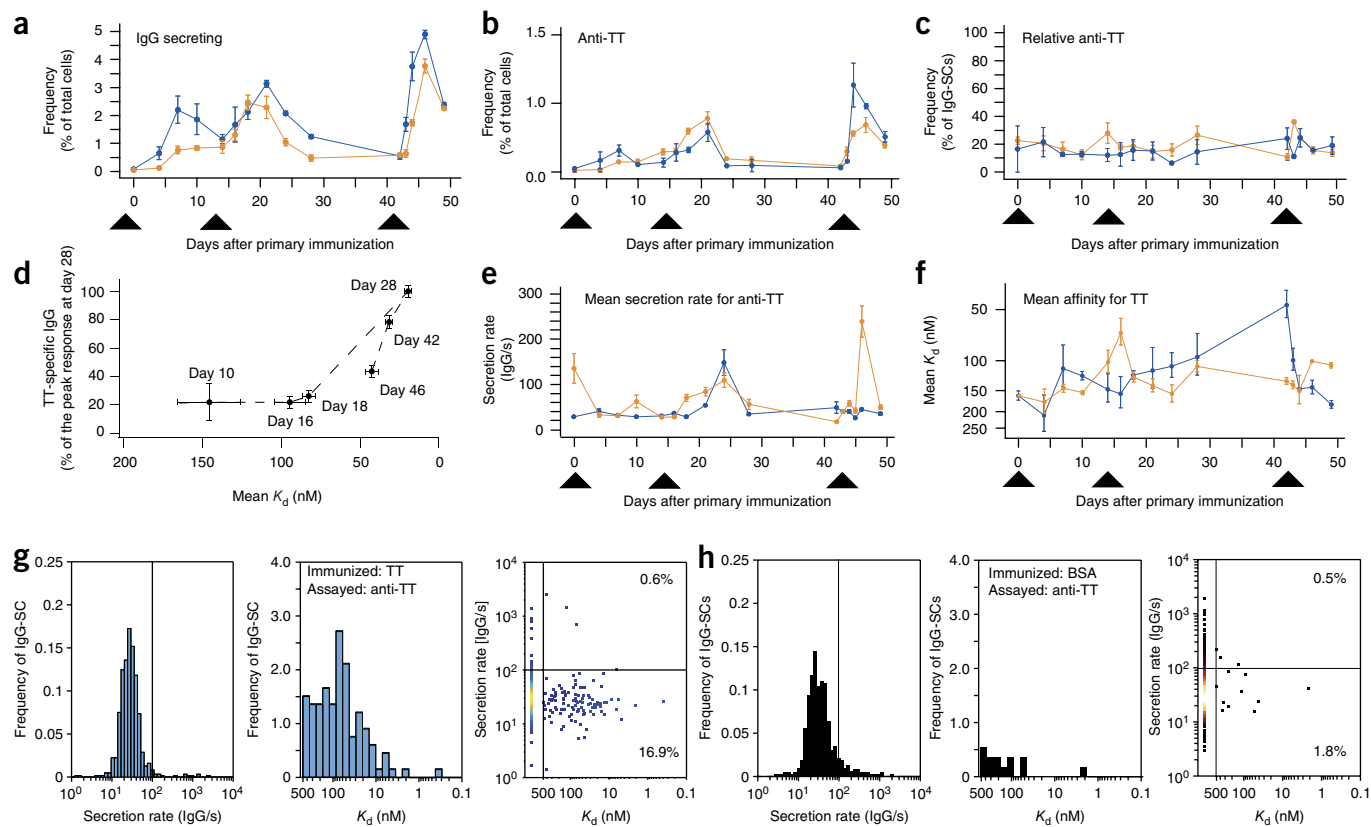


Figure 2 *Ex vivo* measurement of spleen and bone marrow single-cell IgG secretion rates and affinities using DropMap. (**a–f**) Time course analyses of B-cell-enriched cell suspensions from the spleen (orange) and bone marrow (blue) of TT-immunized mice (cell suspensions from three individual mice analyzed per time point). Black triangles below the x-axes indicate time points of immunization; error bars represent the s.e.m. Frequency of IgG-secreting cells (**a**) or anti-TT IgG-secreting cells (**b**) in B-cell-enriched populations. (**c**) Relative frequency of anti-TT IgG-secreting cells (ratio of the frequency of cells secreting anti-TT IgG to the frequency of total IgG-SCs). (**d**) Time course of mean serum IgG affinity for TT and specific IgG as percentage of the peak response at day 28, measured by SPR. Anti-TT IgG was undetectable before day 10. Mean secretion rates (**e**) and mean K_d for TT (**f**) of non-polyspecific anti-TT IgG-secreting cells. Pooled data from spleens of three TT-immunized mice (**g**) or three BSA-immunized mice (**h**) euthanized on day 18 and assayed using the anti-TT bioassay. Distributions of single-cell IgG secretion rates (left), of affinities for TT (K_d , middle), or dot plots of secretion rate vs. affinity for each individual cell (right).

We also compared spleen IgG-SCs from three TT-immunized and three bovine serum albumin (BSA)-immunized mice (identical immunization schedule) at day 18 (**Fig. 2g,h**, **Supplementary Notes**, supplementary fig. 12 and supplementary table 5). We found similar frequencies of IgG-SCs ($2.5 \pm 0.5\%$ and $2.4 \pm 0.4\%$, respectively) with similar secretion rate distributions (mean values 86 ± 23 IgG/s and 74 ± 26 IgG/s, respectively). As expected, the frequency of IgG-SCs producing non-polyspecific anti-TT IgG in BSA-immunized mice ($2.4 \pm 0.5\%$) was lower than in TT-immunized mice ($18.5 \pm 1.8\%$), but only by eightfold. The frequency of IgG-SCs producing non-polyspecific anti-BSA IgG in TT-immunized mice was in the same range ($5.7 \pm 0.5\%$), and is over tenfold higher than the frequency of false positives (0.45%) calculated by analyzing a CHO cell line expressing an antibody against TT (TT7) for binding to BSA (**Supplementary Notes**, supplementary table 6). Thus, a substantial number of IgG-SCs produce cross-reactive antibodies that bind an antigen unrelated to the immunogen. TT-binding IgG was undetectable by serum SPR measurements in BSA-immunized mice, and BSA-binding was undetectable by serum SPR measurements in TT-immunized mice. However, serum titer represents the integral of secretion over time for IgG-SCs in all anatomical compartments, whereas single-cell analysis is a snapshot of antibody secretion at a specific time within spleen and bone marrow, and it could be that

the cells we observe secreting cross-reactive IgG contribute little to the circulating serum IgG pool.

In the TT-immunized mice the frequency of anti-TT IgG-SCs declined rapidly after the peak following secondary immunization and boost in spleen and bone marrow. In contrast, serum titers of anti-TT IgGs remained high after peaking following the secondary immunization and boost (**Supplementary Notes**, supplementary fig. 10), including during an 18-d period (days 24–42) where very few ($\leq 0.2\%$) cells were secreting anti-TT IgGs (**Fig. 2b**). These results were confirmed using SPR, where TT-specific IgG became detectable at only day 10 (i.e., it was undetectable at days 4 and 7), and the TT-specific IgG peaked 14 d after the secondary immunization (day 28), remaining high until day 42 (**Fig. 2d**). Since the serum half-life of IgGs in mice is 4–8 d²⁷, this suggests that the serum titer could be maintained by a reservoir of IgG-SCs niching outside the spleen and bone marrow in other anatomical compartments. Adding to this notion, the changes in mean IgG secretion rates in spleen and bone marrow were modest and do not appear to compensate for the contraction of the anti-TT IgG-SCs reservoir in these tissues (**Fig. 2e** and **Supplementary Notes**, supplementary figs. 13 and 14). Whereas in spleen the mean secretion rates increased after each immunization, reaching a maximum 4 d after the boost (day 46), in bone marrow they remained low, except for a small peak after the second immunization

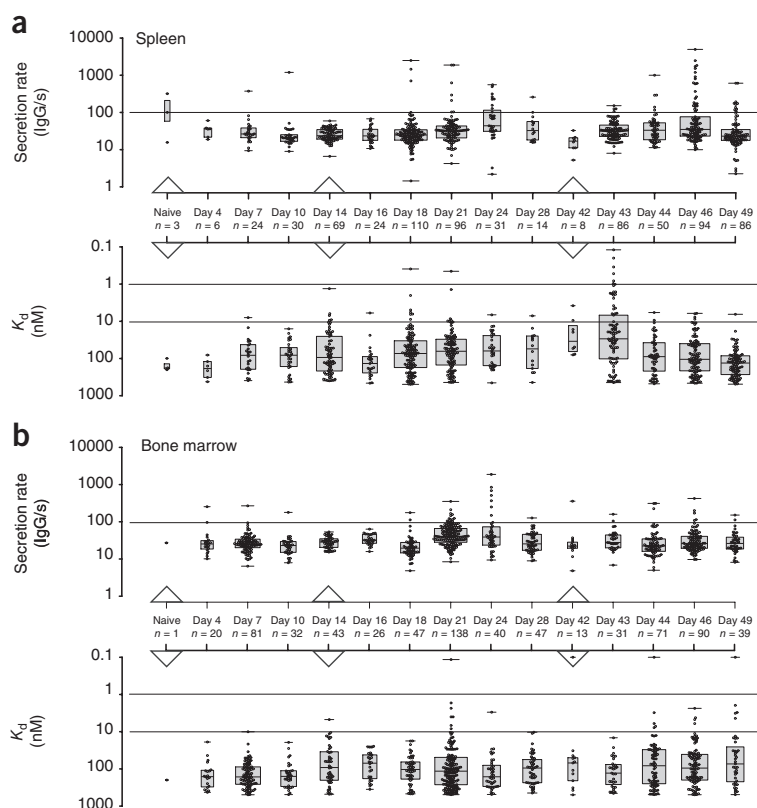


Figure 3 Evolution of single-cell secretion rates and affinities of anti-TT IgG-secreting cells over the time course of immunization. **(a)** Spleen ($n = 731$ among 318,695 cells analyzed). **(b)** Bone marrow ($n = 719$ among 272,899 cells analyzed). Data were pooled from three TT-immunized mice for each time point. Each dot represents a single anti-TT IgG-secreting cell. The widths of the boxes in the box plots are proportional to the square roots of the number (n) for each data point, middle line is the median, upper and lower box are quartiles, and the maximum and minimum values are represented by short horizontal lines. Continuous horizontal lines indicate the thresholds (top) for high-secreting cells (>100 IgG/s), or (bottom) for high- (<10 nM) and very-high affinities (<1 nM) for the TT antigen. Alternative representations of the data can be found in **Supplementary Notes**, supplementary figs. 17–22, and the data for the individual days can be found in **Supplementary Data 1** and **2**.

(day 24). Large changes in the range of single-cell secretion rates of anti-TT IgGs (≤ 25 -fold) were, however, observed, which at maximum spanned up to 3 logs (from ~ 5 to 5,000 IgG/s; **Fig. 3**). Very similar dynamics were observed for TT-binding and non-binding IgGs with only subtle differences between the spleen and bone marrow. High-IgG secretors (>100 IgG/s) appeared only after the second immunization (day 14) in spleen and bone marrow, and after the boost (day 42), particularly in the spleen (**Supplementary Notes**, supplementary fig. 13). Ultra-high IgG secretors ($>1,000$ IgG/s) appeared in very low numbers, mostly in the spleen, representing a maximum of 0.1% of all cells (day 46).

SPR measurements showed that the mean serum affinity of TT-specific IgG increased sevenfold along the immunization scheme, peaking 14 d after the secondary immunization (day 28) and remaining high until the last measurement at day 46 (**Fig. 2d**). Consistent with this, we observed a modest increase (less than two- to fourfold for bone marrow and spleen) in mean affinity (K_d) of TT-binding IgGs from single-cell analysis IgG-SCs (**Fig. 2f**). We further observed a large increase in the range of affinities measured at the single-cell level after primary and secondary immunization and boost, which at maximum spanned nearly 4 logs (K_d from 0.1–500 nM; **Fig. 3**). The largest fraction of cells secreting high-affinity anti-TT antibodies was found in the spleen 1 d after the boost (day 43), where 26% of anti-TT cells secreted antibodies with $K_d < 10$ nM, and 7% secreted antibodies with $K_d < 1$ nM. However, just 1 d later (day 44), the K_d range had collapsed, with only a small fraction (4%) of cells secreting high-affinity antibodies with $K_d < 10$ nM (0% for $K_d < 1$ nM). Notably,

the peak in the frequency of cells secreting high-affinity antibodies ($K_d < 10$ nM) was 4 d earlier (day 43) than the peak in the frequency of high-secreting cells (>100 IgG/s) (at day 46). In contrast, in the bone marrow the K_d range was low 1 d after the boost (day 43), but increased by almost 2 logs by day 44, and remained high at day 49. After the secondary immunization, the increase in K_d range also occurred later in the bone marrow (day 21) than in the spleen (day 18) (**Fig. 3**). No correlation was observed between IgG secretion rate and K_d at the single-cell level (**Fig. 3** and **Supplementary Notes**, supplementary table 7). Therefore, harvesting splenocytes 2–4 d after the boost (as in most hybridoma protocols^{28,29}) maximizes the number of high-secreting cells recovered, but does not appear optimal to recover IgG-SCs secreting high-affinity IgGs.

DropMap captured the full dynamics of the humoral immune response that were only visible with quantitative, time-resolved, and high-throughput single-cell analysis. After immunization, average IgG secretion rates and affinities increased only modestly, but dramatic increases in the distribution of secretion rates and affinities were observed at the single-cell level (**Supplementary Notes**, supplementary figs. 17–22). There were large increases in both the frequency of IgG-SCs and single-cell secretion rates, whether the IgGs were antigen-specific or not, including after the boost with antigen in the absence of adjuvant, and there was no correlation between IgG secretion rate and affinity, pointing to extensive activation and/or stimulation of bystander B cells. Activation of bystander cells may also contribute to the substantial frequency (2.4–5.7%) of IgG-SCs producing

cross-reactive IgGs that bind to an antigen other than the immunogen³⁰. The adjuvant used (in this case Freund's adjuvant) would not be expected a priori to be responsible for the relatively high frequency of IgG-SCs producing cross-reactive IgGs (i.e., BSA-specific in TT-immunized mice or TT-specific in BSA-immunized mice). Nevertheless, it would be interesting to use the DropMap system to further investigate to what extent cells secreting cross-reactive IgGs can be removed by repetitive boosting with pure antigen, and whether certain adjuvants, for example, more 'neutral' and clinically approved adjuvants like inorganic alum or the Toll-like receptor agonist monophosphoryl lipid A, are better suited to drive a more focused immune response toward a given protein antigen, and result in a higher percentage of IgG-SCs secreting IgGs that bind the immunogen. After both secondary immunization and boost, the spleen showed greater plasticity than the bone marrow, and the peak in the number of cells secreting high-affinity, antigen-specific IgGs, was 3 d later in bone marrow than in spleen. This is in agreement with a model in which B-cell expansion and somatic hypermutation in the spleen generate cells secreting high-affinity IgGs, followed by competitive niching of IgG-SCs in the bone marrow.

As a single-cell secretome analysis tool, DropMap is easily scalable (1 million droplets can be analyzed in a 46 × 46 mm chamber), and can be adapted to screen other cells (e.g., T cells) secreting different molecules (e.g., cytokines). It should prove a useful approach to monitor immune responses during pathology and therapy, to optimize immunization and vaccination protocols, and, by optimizing immunization, choice of lymphoid organ, and timing of B-cell harvest, to facilitate the generation of high-quality monoclonal antibodies.

METHODS

Methods, including statements of data availability and any associated accession codes and references, are available in the [online version of the paper](#).

Note: Any Supplementary Information and Source Data files are available in the online version of the paper.

ACKNOWLEDGMENTS

We would like to thank the Institut Pierre-Gilles de Gennes (IPGG) for use of clean room facilities and the laser engraver (CII08, Axyslaser), and Pfizer for the generous gift of TT-Alexa488, and CHO cell lines secreting TT4, TT7, and TT10. TT11 and TT27 antibodies are Pfizer proprietary antibodies isolated from their collaboration with HiFiBio. We thank Pfizer (M. Holsti, G. Cheung, and W. Somers) as well as HiFiBio Team (A. Gérard, A. Woolfe, M. Reichen, A. Poitou, S. Essonno, R. Kumar, S. Ellouze, K. Gosselin, B. Shen, and C. Brennan) for identification, rapid cloning, and validation of TT11 and TT27 antibodies. This work received support from the French Investissements d'Avenir program under the grant agreements ANR-10-NANO-02, ANR-10-IDEX-0001-02 PSL, ANR-10-LABX-31 and ANR-10-EQPX-34, by the French Agence Nationale de la Recherche (ANR-14-CE16-0011 project DROPMabs), from Région Ile-de-France (DIM NanoK) and by the Institut Carnot Pasteur Maladies Infectieuses. K.E. acknowledges financial support from the 'Fondation Pierre-Gilles de Gennes', and the 'Swiss National Science Foundation' and the 'Society in Science—The Branco Weiss Fellowship'. C.C. acknowledges financial support from CONCYTEC, Peru. We would like to further acknowledge R. Henson for making the dscatter function for Matlab publicly available, M. Spitzer, J. Wildenhain, J. Rappsilber and M. Tyers for BoxPlotR that has been used to create the box plots, and B. Iannascoli (Unit of Antibodies in Therapy and Pathology, Institut Pasteur) for help with antibody production and cell lines.

AUTHOR CONTRIBUTIONS

K.E., A.J., A.D.G., J. Bibette, P.B. and J. Baudry designed the study; K.E., R.C.L.D., A.G., E.B.-L., C.N., A.D.G., J. Bibette and J. Baudry developed the technology; K.E., R.C.L.D., C.E.C., L.B.-R., V.M., G.M., P.E. and A.G. performed the experiments; K.E., A.D.G., P.B. and J. Baudry analyzed the data and wrote the paper.

COMPETING FINANCIAL INTERESTS

The authors declare competing financial interests: details are available in the [online version of the paper](#).

Reprints and permissions information is available online at <http://www.nature.com/reprints/index.html>. Publisher's note: Springer Nature remains neutral with regard to jurisdictional claims in published maps and institutional affiliations.

- Nossal, G.J.V. & Mäkelä, O. Elaboration of antibodies by single cells. *Annu. Rev. Microbiol.* **16**, 53–74 (1962).
- Helmreich, E., Kern, M. & Eisen, H.N. The secretion of antibody by isolated lymph node cells. *J. Biol. Chem.* **236**, 464–473 (1961).
- Hibi, T. & Dosch, H.M. Limiting dilution analysis of the B cell compartment in human bone marrow. *Eur. J. Immunol.* **16**, 139–145 (1986).
- Bromage, E., Stephens, R. & Hassoun, L. The third dimension of ELISPOTS: quantifying antibody secretion from individual plasma cells. *J. Immunol. Methods* **346**, 75–79 (2009).
- Salmon, S.E. & Smith, B.A. Immunoglobulin synthesis and total body tumor cell number in IgG multiple myeloma. *J. Clin. Invest.* **49**, 1114–1121 (1970).
- El Debs, B., Utharala, R., Balyasnikova, I.V., Griffiths, A.D. & Merten, C.A. Functional single-cell hybridoma screening using droplet-based microfluidics. *Proc. Natl. Acad. Sci. USA* **109**, 11570–11575 (2012).
- Mazutis, L. *et al.* Single-cell analysis and sorting using droplet-based microfluidics. *Nat. Protoc.* **8**, 870–891 (2013).
- Radbruch, A. *et al.* Competence and competition: the challenge of becoming a long-lived plasma cell. *Nat. Rev. Immunol.* **6**, 741–750 (2006).
- Eisen, H.N. Affinity enhancement of antibodies: how low-affinity antibodies produced early in immune responses are followed by high-affinity antibodies later and in memory B-cell responses. *Cancer Immunol. Res.* **2**, 381–392 (2014).
- Wine, Y. *et al.* Molecular deconvolution of the monoclonal antibodies that comprise the polyclonal serum response. *Proc. Natl. Acad. Sci. USA* **110**, 2993–2998 (2013).
- Lavinder, J.J. *et al.* Identification and characterization of the constituent human serum antibodies elicited by vaccination. *Proc. Natl. Acad. Sci. USA* **111**, 2259–2264 (2014).
- Nossal, G.J.V. & Lederberg, J. Antibody production by single cells. *Nature* **181**, 1419–1420 (1958).
- Georgioui, G. *et al.* The promise and challenge of high-throughput sequencing of the antibody repertoire. *Nat. Biotechnol.* **32**, 158–168 (2014).
- Tas, J.M. *et al.* Visualizing antibody affinity maturation in germinal centers. *Science* **351**, 1048–1054 (2016).
- Czerkinsky, C.C., Nilsson, L.A., Nygren, H., Ouchterlony, O. & Tarkowski, A. A solid-phase enzyme-linked immunospot (ELISPOT) assay for enumeration of specific antibody-secreting cells. *J. Immunol. Methods* **65**, 109–121 (1983).
- Saletti, G., Çuburu, N., Yang, J.S., Dey, A. & Czerkinsky, C. Enzyme-linked immunospot assays for direct *ex vivo* measurement of vaccine-induced human humoral immune responses in blood. *Nat. Protoc.* **8**, 1073–1087 (2013).
- Clargo, A.M. *et al.* The rapid generation of recombinant functional monoclonal antibodies from individual, antigen-specific bone marrow-derived plasma cells isolated using a novel fluorescence-based method. *MABS* **6**, 143–159 (2014).
- Love, J.C., Ronan, J.L., Grotenbreg, G.M., van der Veen, A.G. & Ploegh, H.L. A microengraving method for rapid selection of single cells producing antigen-specific antibodies. *Nat. Biotechnol.* **24**, 703–707 (2006).
- Jin, A. *et al.* Rapid isolation of antigen-specific antibody-secreting cells using a chip-based immunospot array. *Nat. Protoc.* **6**, 668–676 (2011).
- Köster, S. *et al.* Drop-based microfluidic devices for encapsulation of single cells. *Lab Chip* **8**, 1110–1115 (2008).
- Boitard, L. *et al.* Monitoring single-cell bioenergetics via the coarsening of emulsion droplets. *Proc. Natl. Acad. Sci. USA* **109**, 7181–7186 (2012).
- Anna, S.L., Bontoux, N. & Stone, H.A. Formation of dispersions using "flow focusing" in microchannels. *Appl. Phys. Lett.* **82**, 364–366 (2003).
- Foote, J. & Eisen, H.N. Kinetic and affinity limits on antibodies produced during immune responses. *Proc. Natl. Acad. Sci. USA* **92**, 1254–1256 (1995).
- Poulsen, T.R., Meijer, P.J., Jensen, A., Nielsen, L.S. & Andersen, P.S. Kinetic, affinity, and diversity limits of human polyclonal antibody responses against tetanus toxoid. *J. Immunol.* **179**, 3841–3850 (2007).
- Pilbrough, W., Munro, T.P. & Gray, P. Intracloonal protein expression heterogeneity in recombinant CHO cells. *PLoS One* **4**, e8432 (2009).
- Sigal, A. *et al.* Variability and memory of protein levels in human cells. *Nature* **444**, 643–646 (2006).
- Vieira, P. & Rajewsky, K. The half-lives of serum immunoglobulins in adult mice. *Eur. J. Immunol.* **18**, 313–316 (1988).
- Yokoyama, W.M. *et al.* Production of monoclonal antibodies. *Curr. Protoc. Immunol.* **102**, 205 (2013).
- Greenfield, E.A. *Antibodies: A Laboratory Manual*. 2nd edn. (CSH Press, 2014).
- Bernasconi, N.L., Traggiai, E. & Lanzavecchia, A. Maintenance of serological memory by polyclonal activation of human memory B cells. *Science* **298**, 2199–2202 (2002).

ONLINE METHODS

Observation chamber assembly. For the 2D observation chamber (Fig. 1a and Supplementary Notes, supplementary fig. 1a), we used glass microscopy slides as top and bottom covers (76 × 26 × 1 mm, Marienfeld). Two access holes of 1.5-mm diameter were created in the top glass slide using laser ablation (C180II, Axys Laser). Afterwards, both slides were thoroughly cleaned using soap, water, and ethanol, and the two glass slides were exposed to air plasma (60 W) for 10 min (Femto, Diener Electronics). After plasma treatment, distance setting wire (50- μ m diameter, Omega Engineering Inc.) was placed between the two glass slides. The assembly was fixed by clamps, and UV curable glue (Loctite 3526, Henkel) was introduced between the slides by capillary force to seal the chamber. Afterwards, the assembly was cured by UV exposure (ELC-403, Electro-Lite Corporation). Next, two nanoports (N333-01, Idex) and two neodymium magnets (BY042K&J Magnetics) were attached to the holes and sides, respectively. Subsequently, the surface of the 2D chamber was treated using fluoro-silane (Aquapel, Aquapel). Lastly, the chamber was dried under nitrogen, filled with fluorinated oil (Novac HFE7500, 3M) and sealed until used. The chamber could be reused multiple times. The chamber was cleaned after each experiment by flushing fluorinated oil to remove droplets, and was stored filled until the next use. The procedure resulted in a chamber height of 37 μ m, optimal for observation of 40 pl (42 μ m diameter) droplets.

CHO cell lines. IgG, κ anti-TT 4, 7 and 10 producing CHO cell lines (kindly provided by Pfizer) were cultured in ProCHO 4 (Ozyme) supplemented with 2% Glutamax and 1% Pen/Strep (both ThermoFisher). CHO cell lines were tested for the presence of mycoplasma by PCR (VenorGeM Advance, Minerva biolabs) before the study, and regularly during propagation (see also **Life Sciences Reporting Summary**).

Immunization of mice. BALB-C mice were purchased from Janvier Labs (aged 6–10 weeks at start) and housed in the animal facilities of Institut Pasteur during experimentation (see also **Life Sciences Reporting Summary**). Mice were immunized with 10 μ g formaldehyde-inactivated tetanus toxoid (TT, Reagent Proteins, San Diego) in complete Freund's adjuvant (Sigma F5881) mixed 1:1 with 0.9% (w/v) NaCl (Versylene Fresenius) for primary immunization, in incomplete Freund's adjuvant (Sigma, F5506) mixed 1:1 with 0.9% (w/v) NaCl for secondary immunizations or only in 0.9% NaCl for boosting. For immunizations with BSA, mice were injected with 100 μ g BSA using the same adjuvants. Experiments using mice were validated by the CETEA ethics committee number 89 (Institut Pasteur, Paris, France) under #2013-0103, and by the French Ministry of Research under agreement #00513.02.

Extraction of cells from spleen and bone marrow. Spleen and bone marrow from mice were harvested at the indicated time points of the immunization schedule (represented in Supplementary Notes, supplementary fig. 9). Bone marrow cells were flushed and recovered from both tibias and femurs using MACS buffer made comprising 1 × PBS pH 7.2, 0.5% BSA and 2 mM EDTA (for TT bioassays), or comprising 1 × PBS pH 7.2, 0.2% casein and 2 mM EDTA (for BSA bioassays). Spleen cells were recovered following disassociating using a 40- μ m cell strainer. Both cell suspensions were pelleted at 300g for 5 min, red blood cells lysed with a Tris-buffered ammonium chloride solution (0.16 M NH₄Cl, 0.017 M Tris-HCl), cells washed twice with MACS buffer and resuspended in 3 ml of MACS buffer. On average, 100 million splenocytes and 30 million bone marrow cells were obtained per mouse. These cells were further processed using the Pan B Cell Isolation Kit II (Miltenyi Biotec) according to the manufacturer's protocol on an AutoMACS (Miltenyi Biotec, end volume 1 ml, depletion program). The kit depletes non-target cells by depletion of cells expressing CD3 ϵ , CD4, CD8a, CD49b, Gr-1, and Ter119, and therefore enriches for cells from the B-cell lineage. The protocol yields untouched target cells from the B-cell lineage. For both organs we observed approximately a tenfold enrichment of IgG-SCs, measured by the fraction of IgG-SCs within the droplets.

Titer measurements. Standard anti-TT ELISA was performed on sera collected from all mice used in this manuscript, using 1 μ g/ml TT (Reagent Proteins) for coating maxisorp nunc-immuno plates (Thermo Scientific), 1% BSA (Sigma-Aldrich) for blocking, horseradish peroxidase-labeled anti-mouse

Fc-specific antibody (Bethyl) for detection, OPD (Sigma-Aldrich) for revelation, and 2N H₂SO₄ to stop the reaction. Absorbance was read at 492 nm using a spectrophotometer (Biophotometer, Eppendorf).

Aqueous phase I: preparation of cells for droplet creation. For droplet generation, cellular suspensions were centrifuged (300g, 5 min), and in the case of *ex vivo* cell suspensions, resuspended in 100 μ l MACS buffer (Miltenyi Biotec). To this solution, 5 μ l of Fc receptor blocking reagent (Miltenyi Biotec) was added. After 10 min incubation on ice, the cells were spun at 300g for 5 min, and washed once in DMEM/F12 by centrifugation. For TT bioassays, cells were resuspended in working buffer, comprising DMEM/F12 supplemented with 0.1% Pluronic F68 (diluted from 10% stock), 25 mM HEPES pH 7.4, 5% HyClone Super Low IgG Defined Fetal Bovine serum, and 1% Pen/Strep (all ThermoFisher), so as to achieve a λ (mean number of cells per droplet) of 0.2–0.4. For BSA bioassays, the HyClone Super Low IgG Defined Fetal Bovine serum (containing BSA) was exchanged for KnockOut Serum Replacement (ThermoFisher, #10828010), supplemented with 0.5% human serum albumin (Sigma Aldrich, A0237). Cells were collected using centrifugation (300g, 5 min), washed once and resuspended in working buffer before introducing them into the chamber. Cells were resuspended at a density of around 5–10 × 10⁶/ml, to give an average λ of 0.2–0.4 cells per droplet. As the number of cells per droplet follows a Poisson distribution²⁰, at $\lambda = 0.4$, 67% of droplets are empty, 27% contain one cell, and only 6% contain more than one cell.

Aqueous phase II: beads and reagents. Paramagnetic nanoparticles (Strep Plus, 300 nm, Ademtech) were washed and buffer exchange performed using a magnet following the manufacturer's instructions. The nanoparticles were washed twice with PBS. To reduce the non-specific interaction with proteins the particles were resuspended in 10% pluronic F127 (ThermoFisher, in double distilled H₂O), and sonicated at 4 °C (10 min on a pulsed VWR sonicator cleaner USC300TH) for 15 min. Afterwards, the nanoparticles were collected, the supernatant removed and the particles resuspended in PBS containing 1 μ M CaptureSelect biotin anti-mouse IgG κ (light chain specific) conjugate (ThermoFisher). The mixture was incubated for 1 h at room temperature. The nanoparticles were washed twice with PBS, and finally resuspended in the appropriate volume of working buffer containing fluorescently labeled reporter proteins to give a final concentration 0.9 mg/ml beads. Before use, the stock solutions of fluorescently labeled reporter proteins were spun for 10 min at 4 °C at 25,000g to remove aggregates. Rabbit F(ab')₂ anti-mouse IgG Fc-specific (Alexa647 labeled, Jackson ImmunoResearch) and TT (purified monomer, Alexa488-labeled, one fluorophore per TT monomer, kindly provided by Pfizer) were diluted in working solution to 150 and 50 nM, respectively (resulting in final in-droplet concentrations of 75 and 25 nM, respectively). For experiments assaying cross reactivity and polyreactivity of antibodies, we used a mixture of 25 nM TRITC-labeled BSA (Sigma-Aldrich), 25 nM Alexa555-labeled single-stranded DNA (M_w 12.8 kDa, IDT) and 25 nM PE-labeled IgG anti-human IFN γ (Biolegend) in DMEM/F12 (all final concentrations within the droplet) was used. All fluorescent moieties were added to the working buffer with suspended beads shortly before use, and the solution was stored on ice until used and resuspended thoroughly.

Droplet creation and chamber filling. Droplets were created by hydrodynamic flow-focusing²² on a microfluidic device with a nozzle 25 μ m wide, 40 μ m deep, and 40 μ m long (Fig. 1a), fabricated using soft-lithography in poly-(dimethylsiloxane) (PDMS)³¹, as previously described⁷. The continuous phase comprised 2% (w/w) 008-FluoroSurfactant (RAN Biotechnologies) in HFE7500 fluorinated oil. Aqueous phases I and II (cells or calibration antibodies, and beads with reagents, respectively) were co-flowed on-chip. The flow rates (around 800 μ l/h for oil, and 100 μ l/h for each aqueous solution, supplied using a neMESYS syringe pump, Cetoni) were adjusted to create droplets of 40 ± 3 pl (diameter 42.5 ± 0.9 μ m, n ≈ 3,000, measured by image analysis). During droplet creation, the cellular suspension was cooled using iced water to inhibit antibody secretion. Shortly after creation, the monodisperse droplets were passed through a ring magnet (H250H-DM, Amazing Magnets) to force the nanoparticles to form beadlines. The emulsion was either directly injected into the 2D chamber system, or collected in a 1.5-ml Eppendorf tube containing fluorinated oil with 0.1% (w/w) 008-FluoroSurfactant, either on ice

(cell experiments) or at room temperature (cell-free experiments). If collected in a tube, the droplets were diluted 1:1 using fluorinated oil containing 0.1% (w/w) 008-FluoroSurfactant before introduction into the observation chamber using a custom-made PDMS valve. Droplets were reinjected into the chamber using a flow rate of 750 $\mu\text{l/h}$. After chamber filling was complete resulting in a water volume fraction of >40%, the chamber was gently closed and mounted onto a fluorescence microscope (Ti Eclipse, Nikon).

Data acquisition and analysis. Imaging was performed using a Nikon (Ti-E) inverted microscope with a motorized stage. Excitation light was provided by a LED source (SOLA light engine, Lumencor Inc.). Fluorescence for the specific channels were recorded using appropriate band-pass filters (GFP and TRITC filter sets, Nikon, and Cy5 filter set, Semrock) and camera settings (Orca R2, Hamamatsu) at room temperature (25 °C) and ambient oxygen concentrations. Images were acquired using a 10 \times objective (NA 0.45). An array of 10 \times 10 images were acquired for each experiment, every 7.5 min in all channels over 37.5 min (five measurements total). The array was imaged in one channel throughout, and the channel was changed afterwards and the array reimaged. The images were then analyzed using a custom Matlab script (Mathworks). Droplets were detected by using Hough transformation³² on the contrast between droplets and outer phase in brightfield pictures. The droplet mask generated was overlaid onto the fluorescence images, and each droplet was analyzed separately. Within each detected droplet, the signal was averaged over the direction of the magnetic field and normalized to the number of pixels. Next, the maximum and mean fluorescence were calculated from these averaged results. The maximal intensity was normally found on the beadline, and averaging in the field direction allowed integration of the fluorescent signal over the whole beadline. Data were then exported to Excel (Microsoft), and, for each time point, the ratio of the maximal signal (on the beadline) and the average signal over the whole droplet was calculated. For further analysis, only droplets showing an increase in relocation of the anti-IgG Fc-specific secondary antibody (Alexa647 labeled; red fluorescent) above a threshold (equivalent to 1.2 nM after 37.5 min, i.e. around four molecules/s) were selected. Droplets with ratios of maximum red fluorescence to mean red fluorescence above 1.7, higher than the maximum observed with purified IgG (Fig. 1d; see also Supplementary Notes, supplementary fig. 11), which likely correspond to polyspecific IgGs (antibodies that bind to multiple structurally unrelated antigens), were excluded from the analysis. Each droplet was further visually controlled for cellular accumulation of fluorescence, pixel errors, insufficiently long beadlines or dust particles, or the presence of multiple cells, and if any such characteristic was detected in a given droplet, it was excluded from the analysis.

Calculation of the secretion rate. To calculate the IgG secretion rates from the raw data, the ratio of red fluorescence (anti-IgG Fc specific channel) bound to the beadline and mean red fluorescence in the whole droplet was used. These ratios were converted to IgG concentrations using a calibration curve (Fig. 1d) prepared using a purified anti-TT IgG (TT7, Supplementary Notes, supplementary table 2) with K_d of 8 nM (Supplementary Notes). The secretion rate within each droplet was calculated by extracting the change in concentration from one time point to the next (up to four values per droplet), and dividing by the time interval. The binding capacity of the beads was found to be equivalent

to around 75 nM IgG (Fig. 1d), and therefore secretion rates were only calculated for IgG concentrations ≤ 50 nM, higher concentrations being excluded from the determination.

Calculation of the dissociation constant. Knowing the concentration of secreted IgG in each drop from the relocation within the anti-IgG(Fc) channel (red fluorescence), affinity (K_d) was calculated from the respective relocation within the antigen (green fluorescence) channel (for more information, please refer to the Supplementary Notes). The theoretical model (see Supplementary Notes) predicts that the K_d of the IgG for the antigen can be determined from the slope of the curve defined by the ratio of relocation of anti-IgG(Fc) to the beadline (beadline red fluorescence/mean droplet red fluorescence) versus the relocation of antigen to the beadline (beadline green fluorescence/mean droplet green fluorescence), measured at different concentrations of IgG. Dissociation constants were calculated for IgG concentrations ≤ 50 nM, higher values were being excluded from the slope determination.

Real-time surface plasmon resonance (SPR). SPR experiments were performed on a Biacore T200 instrument (GE Healthcare) at 25 °C. 8,000–8,500 RU (1 RU ~ 1 pg/mm²) of polyclonal rabbit anti-mouse antibodies reacting with all mouse IgG subclasses (Mouse Antibody Capture Kit, GE Healthcare) were covalently immobilized on the four flow cells of a carboxymethylated dextran CM5 sensorchip (GE Healthcare) according to the manufacturer's instructions. The instrument was then equilibrated thoroughly in PBS supplemented with 0.2 mg/ml BSA.

For each experiment, IgGs from sera harvested on the same day (days 4, 7, 10, 16, 18, 28, 42, and 46) from three individual, immunized mice were captured at a density of 900–1,200 RU on three different flow cells. As a reference, IgGs from a naive mouse were captured at the same density on the fourth flow cell. The binding of TT to this IgG matrix was monitored in real time by injecting purified TT (seven concentrations ranging from 7.8 to 500 nM) for 15 min at a flow rate of 20 $\mu\text{l/min}$ on all four flow cells. The dissociation of TT was then followed for 15 min, before regenerating the surfaces with 3 \times 3 min injections of Gly-HCl pH 1.7. The SPR signals were processed by double-referencing, that is, the raw signals from the reference surface were subtracted from those for the other three, as well as the signals obtained for the injections of blank samples (running buffer).

The association and dissociation profiles were analyzed using the Biacore T200 evaluation software (v 3.0), assuming a 1:1 simple Langmuir interaction mechanism, yielding an average equilibrium dissociation constant (K_d) for the anti-TT IgGs contained in each serum. The percentage of TT-specific IgGs in each serum was determined by calculating the ratio between the TT signal obtained at saturating concentration (R_{max}) and the signal of total IgGs captured from the serum. The data are shown as the relative fraction of the maximal answer at day 28 (Fig. 2d).

Data availability. All data are included with the paper.

31. Duffy, D.C., McDonald, J.C., Schueller, O.J.A. & Whitesides, G.M. Rapid prototyping of microfluidic systems in poly(dimethylsiloxane). *Anal. Chem.* **70**, 4974–4984 (1998).
32. Duda, R.O. & Hart, P.E. Use of the Hough transformation to detect lines and curves in pictures. *Commun. ACM* **15**, 11–15 (1972).

Life Sciences Reporting Summary

Nature Research wishes to improve the reproducibility of the work that we publish. This form is intended for publication with all accepted life science papers and provides structure for consistency and transparency in reporting. Every life science submission will use this form; some list items might not apply to an individual manuscript, but all fields must be completed for clarity.

For further information on the points included in this form, see [Reporting Life Sciences Research](#). For further information on Nature Research policies, including our [data availability policy](#), see [Authors & Referees](#) and the [Editorial Policy Checklist](#).

▶ Experimental design

1. Sample size

Describe how sample size was determined.

No statistical method was used. The study is exploratory, but we used the standard animal experiment size of 3 mice per group, as recommend as a minimum by our ethics committees.

2. Data exclusions

Describe any data exclusions.

No animals and/or data were excluded.

3. Replication

Describe whether the experimental findings were reliably reproduced.

We replied certain data points of our study and found similar results that were found to be non-significantly different in terms of numbers and distributions.

4. Randomization

Describe how samples/organisms/participants were allocated into experimental groups.

No method of randomization was chosen.

5. Blinding

Describe whether the investigators were blinded to group allocation during data collection and/or analysis.

No blinding was performed. All mice received the same treatment, as this study is a kinetic study on a particuar immunization.

Note: all studies involving animals and/or human research participants must disclose whether blinding and randomization were used.

6. Statistical parameters

For all figures and tables that use statistical methods, confirm that the following items are present in relevant figure legends (or in the Methods section if additional space is needed).

n/a Confirmed

- The exact sample size (n) for each experimental group/condition, given as a discrete number and unit of measurement (animals, litters, cultures, etc.)
- A description of how samples were collected, noting whether measurements were taken from distinct samples or whether the same sample was measured repeatedly
- A statement indicating how many times each experiment was replicated
- The statistical test(s) used and whether they are one- or two-sided (note: only common tests should be described solely by name; more complex techniques should be described in the Methods section)
- A description of any assumptions or corrections, such as an adjustment for multiple comparisons
- The test results (e.g. P values) given as exact values whenever possible and with confidence intervals noted
- A clear description of statistics including central tendency (e.g. median, mean) and variation (e.g. standard deviation, interquartile range)
- Clearly defined error bars

See the web collection on [statistics for biologists](#) for further resources and guidance.

► Software

Policy information about [availability of computer code](#)

7. Software

Describe the software used to analyze the data in this study.

The software used was a custom-written Matlab script, able to detect each droplet as well as determining mean and maximal fluorescence within each droplet.

For manuscripts utilizing custom algorithms or software that are central to the paper but not yet described in the published literature, software must be made available to editors and reviewers upon request. We strongly encourage code deposition in a community repository (e.g. GitHub). *Nature Methods* [guidance for providing algorithms and software for publication](#) provides further information on this topic.

► Materials and reagents

Policy information about [availability of materials](#)

8. Materials availability

Indicate whether there are restrictions on availability of unique materials or if these materials are only available for distribution by a for-profit company.

Restrictions apply for the tetanus-toxoid Alexa488 conjugate that was prepared by Pfizer and was received as a generous gift for this study, along with the CHO cell lines secreting TT4, TT7 and TT10. TT11 and TT27 antibodies are Pfizer proprietary antibodies isolated from their collaboration with HiFiBio.

9. Antibodies

Describe the antibodies used and how they were validated for use in the system under study (i.e. assay and species).

Sequences for the antibodies can be found in the Supplementary Note. Species and specificity of the antibodies was confirmed by ELISA measurements.

10. Eukaryotic cell lines

a. State the source of each eukaryotic cell line used.

CHO parental cell line as well as HEK293T cell line were obtained from ATCC.

b. Describe the method of cell line authentication used.

The cells were used as an transfection host for antibody production, their identity was confirmed visually using light-microscopy after receipt and before experiments.

c. Report whether the cell lines were tested for mycoplasma contamination.

Yes, CHO cell lines were tested for the presence of mycoplasma by PCR (VenorGeM Advance, Minerva biolabs) before the study, and regularly during propagation.

d. If any of the cell lines used are listed in the database of commonly misidentified cell lines maintained by [ICLAC](#), provide a scientific rationale for their use.

None to declare.

► Animals and human research participants

Policy information about [studies involving animals](#); when reporting animal research, follow the [ARRIVE guidelines](#)

11. Description of research animals

Provide details on animals and/or animal-derived materials used in the study.

BALB-C mice were purchased from Janvier Labs (age 6-10 weeks at start) and housed in the animal facilities of Institut Pasteur during experimentation.

Policy information about [studies involving human research participants](#)

12. Description of human research participants

Describe the covariate-relevant population characteristics of the human research participants.

None to declare.